Journal of Power Sources 186 (2009) 515–520

Contents lists available at ScienceDirect

Journal of Power Sources

journal homepage: www.elsevier.com/locate/jpowsour

Superior hydrogen absorption and desorption behavior of Mg thin films

Jianglan Qu[a], Yuntao Wang[a], Lei Xie[a], Jie Zheng[a], Yang Liu[a], Xingguo Li[a,b,*]

[a] Beijing National Laboratory for Molecular Sciences (BNLMS), The State Key Laboratory of Rare Earth Materials Chemistry and Applications, College of Chemistry and Molecular Engineering, Peking University, Beijing 100871, China
[b] College of Engineering, Peking University, Beijing 100871, China

ARTICLE INFO

Article history:
Received 5 April 2008
Received in revised form 13 October 2008
Accepted 15 October 2008
Available online 5 November 2008

Keywords:
Hydrogen storage
Magnesium thin films
Hydrogen desorption

ABSTRACT

Pd-capped Mg films prepared by magnetron sputtering achieved complete dehydrogenation in air at room temperature and behaved as favorable gasochromic switchable mirrors. Their cyclic hydrogen absorption and desorption kinetics in air were investigated by using the Bruggeman effective medium approximation. The overall activation energy was 80 kJ mol^{-1}, while the reaction orders controlling desorption were deduced to be $n = 2$ at 328 K and $n = 1$ at lower temperatures by analyzing the transmittance data. The hydrogen diffusion coefficient and the corresponding activation energy were calculated by electrochemical measurements. Mg thin films exhibited the smaller activation energy and remarkable diffusion kinetics at room temperature which implied potential applications in smart windows.

1. Introduction

Hydrogen storage materials have attracted intensive attention for the increasing demands on energy consumption and environment protection. Mg is considered as a promising hydrogen storage material for automotive applications due to its high capacity (7.6 wt% of hydrogen), lightweight and low cost. However, thermodynamics indicate that hydrogen desorption of the bulk MgH_2 only takes place at temperatures above 600 K, which is a major impediment to application [1]. Recently, tremendous efforts have been devoted to decrease the operation temperature and improve the desorption kinetics by preparing nano-composites, due to their high chemical activity and fast diffusion ability [2,3]. Thin film technique is a powerful method to investigate the interaction between Mg and hydrogen because the composition, interface and crystallinity can be well defined on the nano-scale [4,5]. Thus, various attempts have been undertaken to study the hydrogen storage properties of Mg thin films [6–9]. Moreover, though the hydrogen absorption properties have been the subject of much study, the desorption behavior requires clarification. Results show that drastic reductions in the desorption temperatures have been found in Pd/Mg films at 473 K [10] and Pd/Mg/Pd films around 373 K [11]. Doping Mg with catalysts, such as Nb or Pd, could also improve the desorption kinetics at higher temperatures in vacuum [12,13]. However, desorption behavior of Pd-capped pure Mg films at moderate conditions has rarely been verified.

In addition, the term "switchable mirror" has been used to describe the spectacular optical and electrical changes during hydrogen absorption and desorption. In 1996 Huiberts et al. first discovered that Y and La thin films exhibited optical switching from the mirror state to the transparent state [14]. Similar behavior was subsequently found in Mg-rare-earth films and magnesium-transition-metal alloys, such as MgNi and MgTi films [15–19]. These intriguing thin films could potentially be applied as displays, hydrogen sensors, smart windows and solar absorbers [20,21]. Yoshimura et al. have developed all-solid-state switchable devices, which exhibit excellent gasochromic switching properties [22–24]. MgNi alloy films, with a wide optical-modulation range, could be applied as energy efficient windows [25,26]. Moreover, the color neutral Mg–Ti–H thin films are suitable for solar collectors, as well as smart windows and hydrogen sensors [18,20,27]. Pd-capped pure Mg films could also exhibit drastic optical and electrical changes upon exposure to hydrogen [28,29].

However, few results in the literatures indicate that hydrogen desorption of pure Mg films in air at room temperature is possible, which is an important step toward the practical application [30,31]. Therefore, it is significant to investigate the detailed structural, optical and electrical changes during the hydrogen absorption and desorption process at room temperature in order to understand the interaction mechanism between Mg and hydrogen. It is convenient to prepare pure Mg films and construct a corresponding

* Corresponding author at: Beijing National Laboratory for Molecular Sciences (BNLMS), The State Key Laboratory of Rare Earth Materials Chemistry and Applications, College of Chemistry and Molecular Engineering, Peking University, Beijing 100871, China. Tel.: +86 10 62765930; fax: +86 10 62765930.
E-mail address: xgli@pku.edu.cn (X. Li).

0378-7753/$ – see front matter © 2008 Elsevier B.V. All rights reserved.
doi:10.1016/j.jpowsour.2008.10.079

simple film model to deduce the kinetics mechanism. Moreover, investigation of the kinetic parameters is of guidance to explore advanced Mg-based hydrogen storage materials.

Herein, the hydrogen absorption and desorption properties of Pd-capped Mg thin films were investigated by monitoring the changes in structure, transmittance and resistance. The reaction kinetics was analyzed with a nucleation and growth mechanism by assuming a double layer model. The kinetic parameters, overall activation energy, hydrogen diffusion coefficient and the corresponding activation energy were all calculated to trace the superior hydrogen absorption and desorption behavior of Mg thin films.

2. Experimental

Pd-capped Mg thin films were prepared by a custom designed direct current (DC) magnetron sputtering system with a background pressure of around 2×10^{-4} Pa. Mg layer with 100 nm thickness was firstly deposited onto Si (1 0 0) wafers, glass and ITO-coated glass (indium tin oxide) substrates by DC sputtering using a Mg (99.99%) target. The discharge power was 50 W and the argon (99.99%) pressure was 0.8 Pa. Then a 10 nm Pd layer was coated on top of the Mg layer by DC sputtering using a Pd (99.99%) target. The discharge power was 45 W and the argon pressure was 0.8 Pa. The Pd cap layer is necessary to protect Mg against oxidation and to promote hydrogen dissociation. The deposition rates of Mg and Pd were 0.26 nm s^{-1} and 0.33 nm s^{-1}, respectively. After deposition, the samples were transferred into a steel chamber which was evacuated to 10^{-3} Pa later. Then it was loaded with 0.1 MPa hydrogen (99.99%) and was maintained at 353 K for 4 h.

The structures of the samples were identified by powder X-ray diffraction (XRD) (Rigaku D/max-2000) using monochromated Cu Kα radiation and ⟨theta⟩–2⟨theta⟩ scan. Film thicknesses were determined by cross-section scanning electron microscopy (SEM) observations using a Hitachi S4800 at 10 kV. Optical transmission measurements at 298 K were performed by using a UV–vis recording spectrophotometer (Shimadzu UV-2401PC) with a dual beam measurement system. The UV–vis transmission spectra at higher temperatures were measured with Shimadzu UV-3100 spectrometer. The changes in resistance were recorded in a gas loading cell equipped with a four-probe resistance measurement, monitored by a Keithley 2000 digital multimeter. The diffusion coefficient of the Mg films deposited on ITO-coated glass substrates was determined by the electrochemical multi-potential steps method in 6 M KOH solution. Platinum foil and Hg/HgO were used as the counter and reference electrode, respectively. The fast rate (100 mV s^{-1}) cyclic voltammogram was applied to clean the surface prior to measurements. The Mg film electrode was firstly held at a cathodically polarized potential (−1.10 V vs Hg/HgO) for 2 h and subsequently switched to an anodically polarized potential (−0.5 V vs Hg/HgO) for another 2 h.

3. Results and discussion

3.1. Structural characterization

The XRD patterns of Mg thin films during hydrogen absorption and desorption cycles are shown in Fig. 1. In the as-prepared samples, the peak around 34.6° was the preferential growth orientation of Mg (0 0 2), while the broad peak around 40.0° was attributed to Pd (1 1 1). Upon exposure to 0.1 MPa H_2 at 353 K for 4 h, the Mg (0 0 2) peak disappeared and the MgH_2 (1 1 0) peak became significant. Subsequently dehydrogenated at 298 K in ambient air, the Mg (0 0 2) peak reappeared and the sample transformed completely from rutile β-MgH_2 to h-Mg. The Mg (1 0 1) peak also appeared

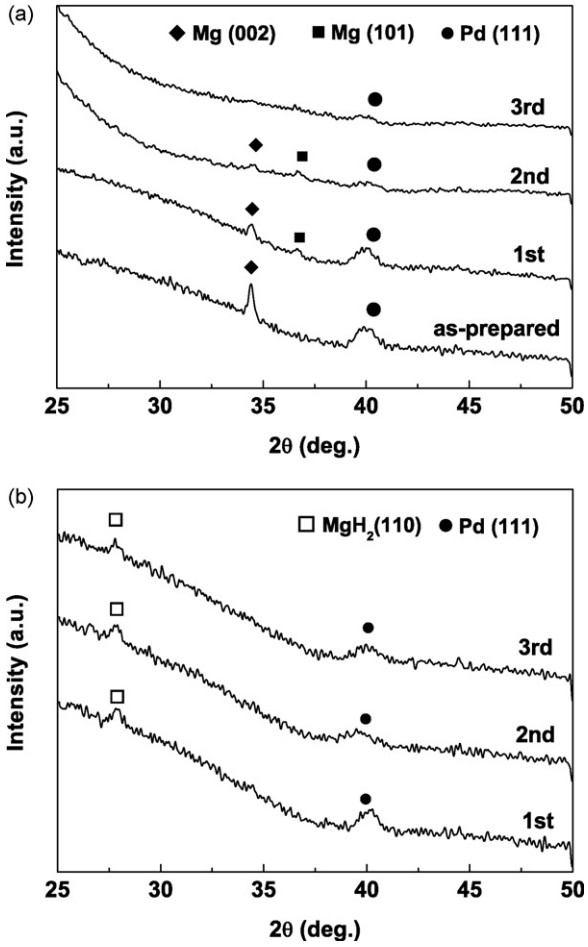

Fig. 1. (a) XRD patterns of Mg thin films as-prepared and during the hydrogen desorption cycles in air at 298 K. (b) XRD patterns of Mg thin films during the hydrogen absorption cycles in 0.1 MPa H_2 at 353 K for 4 h.

at 36.5°, suggested that the preferential orientation of the (0 0 2) direction was attenuated and the restructured Mg formed. The samples could absorb–desorb hydrogen reversibly, although the peaks became weaker and broader with the increasing cycle numbers, due to the strong hydrogen induced stress during the structure change. According to Debye–Scherrer analysis, the crystalline size decreased from 36 nm for the as-prepared sample to 22 nm after the first cycle.

3.2. Optical switching properties

The photographs of Mg films during hydrogen absorption and desorption are shown in Fig. 2. The image of the camera was reflected on the as-prepared metallic film. The red logo of Peking University in Chinese characters behind the sample could not be seen entirely. After fully hydrogenation at 353 K, the whole logo was seen clearly through the transparent film, which indicated that a visible metal–insulator transition took place due to the hydrogenation. Upon dehydrogenated at ambient air, the highly reflecting shiny film obstructed the view of the logo again.

The samples presented optical switching properties. Fig. 3 illustrates the optical transmittance changes at 500 nm with respect to the exposure time during desorption cycles in ambient air. As shown in the figure, the transmittance decreased immediately once the samples were exposed to air at room temperature. The film

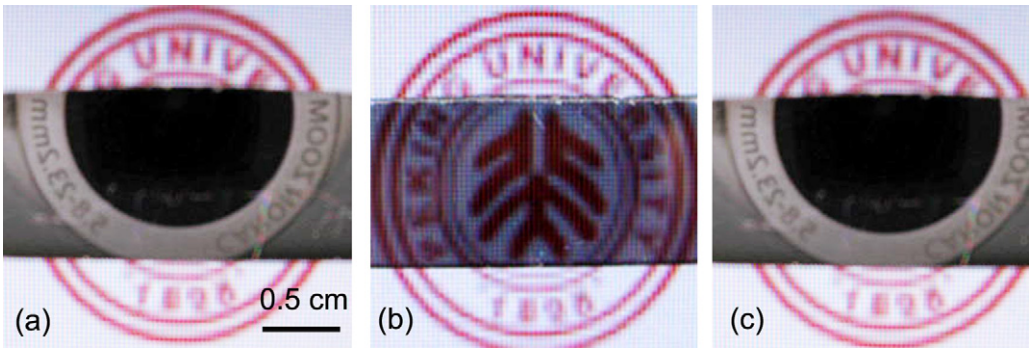

Fig. 2. Photographs of Mg thin films during hydrogen absorption and desorption. The red logo belongs to Peking University. (a) As-prepared sample (b) after hydrogenation in 0.1 MPa H_2 at 353 K for 4 h (c) after dehydrogenation in air at 298 K for 5 h.

dehydrogenated in air at 298 K, which were attributed to the surface reactions on the Pd layer. The hydrogen could react with oxygen to form an OH group and eventually a water molecule, which desorbed from the surface [32]. According to Lambert–Beer's law, the logarithm of the optical transmission $\ln(T/T_0)$ is found to vary linearly with the hydrogen concentration in the film, where T_0 is the maximum transmittance of the film after fully hydrogenation [33]. Since the slopes of the transmittance curves described the desorption rates of the hydride in the initial dehydrogenation process, a deterioration of desorption rates with the increasing cycles were observed in Fig. 3. The failure of the Pd cap layer and the formation of magnesium oxide at the outermost surface were the major causes of the degradation [23,34]. The reason could be that alloying between Mg and Pd during cycling results in the interdiffusion of the two elements, and the nonreversible hydride forms and leads to partially dehydrogenation [35,36]. The encapsulation of the Pd catalyst was usually observed during cycling of switchable mirrors and caused by strong metal–support interaction (SMSI) [37,38]. The same degradation phenomenon was also found in other Mg-based systems [23,34].

3.3. Electrical resistance

The time dependent resistance during hydrogen absorption and desorption provided information about the kinetic properties as well as hydrogen-induced changes of electrical properties. For modeling the electrical properties of a mixture of two materials A and B during hydrogen absorption, we could apply the Bruggeman effective medium approximation [16]:

$$\frac{f_A(\rho_A-\rho)}{L\rho+(1-L)\rho_A}+\frac{f_B(\rho_B-\rho)}{L\rho+(1-L)\rho_B}=0 \quad (1)$$

where f_A and f_B are the corresponding volume fractions ($f_A+f_B=1$) and L is the geometric factor ($L=1/3$ for spherical inclusions). To simulate the experiments, we assumed a double layer model with 20 nm Pd–Mg composite layer with the resistivity of 75 μΩ cm in parallel with the 90 nm Mg–MgH_2 layer. Mg had a resistivity of 6.5 μΩ cm and the resistivity of MgH_2 was assumed to be 10 mΩ cm. The time dependent volume fraction of MgH_2 is shown in Fig. 4. The absorption rates increased with the increasing cycle numbers. For example, at the first absorption cycle, f_d (MgH_2) saturated after exposure to H_2 for 80 min, suggested that the complete transformation from Mg to MgH_2 had almost been achieved. While on the second absorption cycle, the f_d (MgH_2) reached the saturation in only one hour. The explanation could be that hydrogen absorption–desorption induced smaller grain size and more defects which promoted the hydrogen penetration, as proved by XRD [9]. Moreover, at the very beginning process, f_d (MgH_2) during all the cycles increased dramatically because the hydrogen atoms penetrated throughout both the grain boundaries and the metal spheres. Then the hydrogen atoms had to diffuse through the blocking MgH_2 layer beneath the Pd layer and therefore the loading rate reduced [39].

The relative resistance change, R/R_0, which was proportional to the hydrogen concentration in the Mg film, was plotted as a function of the desorption time at different temperatures, shown in Fig. 5

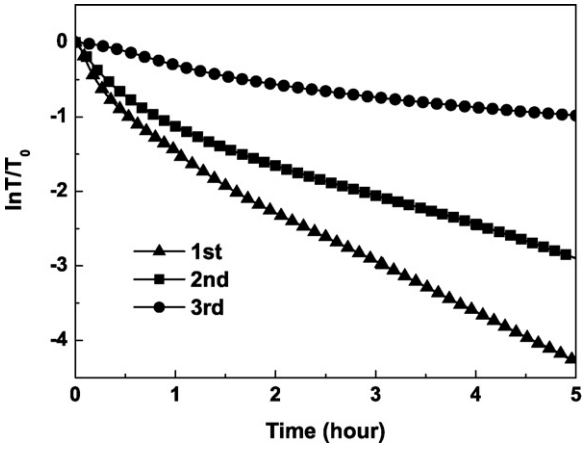

Fig. 3. Optical transmittance change at 500 nm of Mg thin films with respect to the exposure time during desorption cycles in air at 298 K.

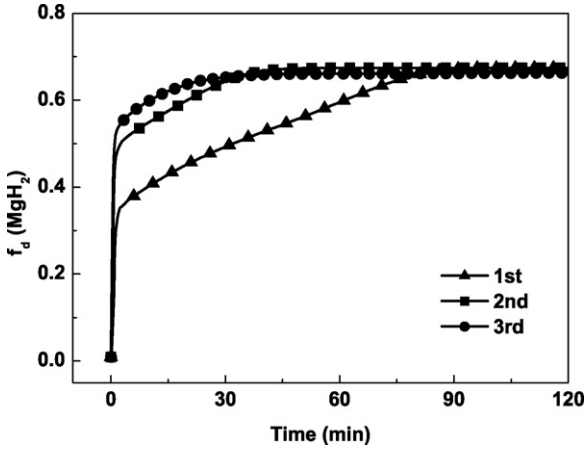

Fig. 4. The volume fraction of MgH_2, f_d (MgH_2), with respect to the hydrogenation time under 0.1 MPa H_2 at 353 K.

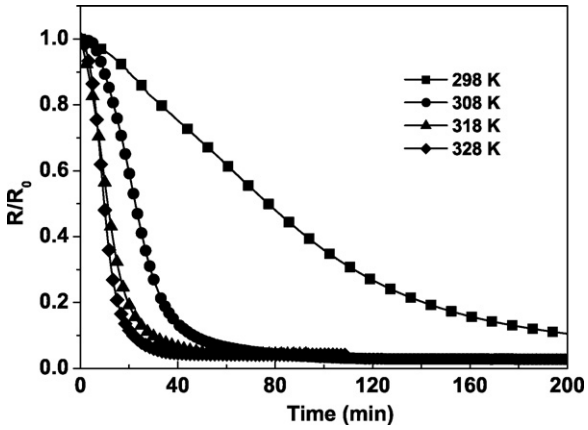

Fig. 5. Relative resistance change of Mg films, R/R_0, during hydrogen desorption at different temperatures in air.

[40]. R_0 is the maximum resistance of the initial hydride film. The resistance decreased upon exposure to air, due to the formation of metallic Mg grains during the dehydrogenation process. While the resistance reached the similar value as that of the as-prepared film and did not change any more after a period of time, indicated that the samples completely transformed to metallic films. As shown in the figure, the hydrogen desorption rates were much improved at higher temperatures in air. At 328 K, the film achieved complete dehydrogenation after merely 30 min. The overall rate was 10 times higher than that at room temperature. This tendency could be suitable for practical use in energy efficient windows, which could transform from the transparent state to the mirror state at hot condition to block sunshine [21].

3.4. Hydrogen desorption kinetics

3.4.1. Activation energy in hydrogen desorption

Faster dehydrogenation kinetics with higher temperatures was clearly visible, as illustrated in Fig. 6 (a). The desorption data had been analyzed by using the Jonhnson–Mehl–Avrami theory [41]. Upon a first-order phase transition, the reacted fraction was given as function of time, by

$$r = 1 - \exp[-(kt)^n] \quad (2)$$

where r is the reacted fraction, t is the desorption time, $k = k(T)$ is the temperature dependent kinetic constant and n is the reaction order. A linear interpolation of the plots, $\ln(-\ln(1-r))$ vs $\ln(t)$, yielded the values of n and k. Since the reacted fractions of thin films were difficult to be measured using the gravimetric and volumetric method, we used the transmittance data to calculate r. According to the Lamber–Beer law, $\ln(T/T_0)$ was a good indicator of the hydrogen concentration [31]. Assuming that it was totally dehydrogenated when the transmittance saturated as a function of time, it was then possible to determine the desorption rates from the slopes of the curves. Hence, the amount of hydride transforms to metal (reacted fraction r) in desorption process could be obtained.

The temperature dependent desorption rates generally followed the Arrhenius type law. From the slopes of the initial experimental data, the overall activation energy of hydrogen desorption was obtained as 80 kJ mol^{-1}, shown in Fig. 6(b). The activation energy deduced from our experiment was lower than the value 94 kJ mol^{-1} obtained in Ni-catalyzed MgH_2 system [42]. The smaller desorption activation energy could be attributed to the catalyst effect of Pd layer and the nanocrystalline structure of the thin films.

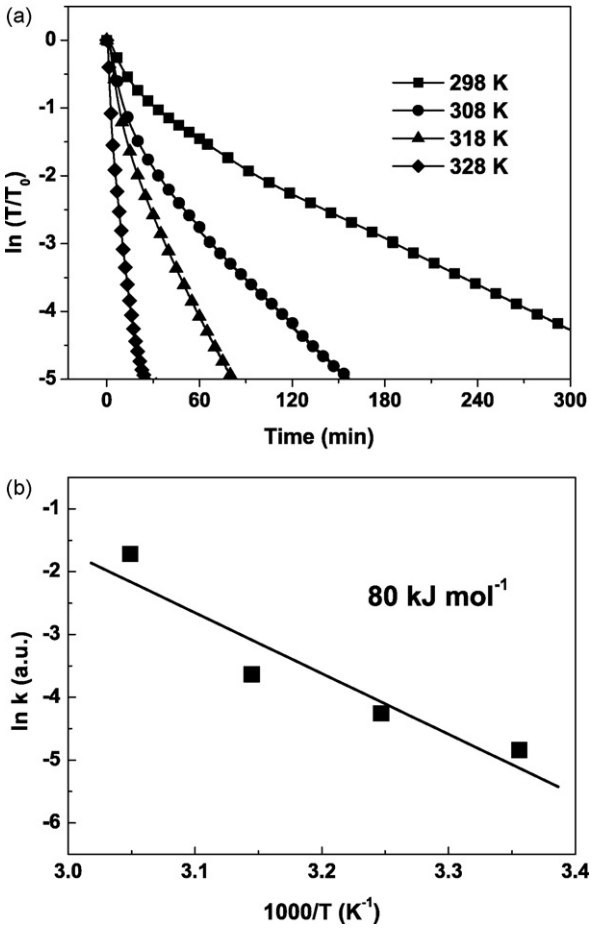

Fig. 6. (a) Relative transmittance change at 500 nm, $\ln(T/T_0)$, with respect to desorption time under different temperatures in air. (b) Arrhenius plots for hydrogen desorption in air. The straight line is the linear fit according to data.

In hydrogen desorption reaction, the transmittance data seemed to follow a nuclear and growth mechanism. The value of the exponent varied from $n = 1$, at 298 K, 308 K and 318 K to $n = 2$ at 328 K. Due to the Pd catalyst, the dissociation rate could be considered as sufficiently fast. Therefore, the $n = 2$ at higher temperature was expected that a constant number of Mg nuclei form very quickly at the beginning of the process. The growth of the nuclei in the film was controlled by a two-dimensional interface process. While the $n = 1$ at lower temperature was expected that the phase transition occured by the one-dimensional growth of a fixed number of Mg grains [43].

3.4.2. Hydrogen diffusion coefficient

Hydrogen diffusion coefficient and the corresponding activation energy are two important parameters in the hydrogen desorption process. Since the diffusion was governed by the Fick's second law with a constant diffusion coefficient, Hagi's model was applied to analyze the current with respect to the discharge time to calculate the hydrogen diffusion coefficient [44,45]. When time is long ($>3L^2/\pi^2 D_H$), the current density could be approximated using the long time expression as

$$J_H = \frac{(C_0 - C^*)D_H}{L^2} \exp\left(\frac{-\pi^2 D_H t}{4L^2}\right) \quad (3)$$

where J_H is the current density, t is the discharge time, D_H is the hydrogen concentration independent diffusion coefficient, L is the thickness of the film electrode, C_0 is the initial hydro-

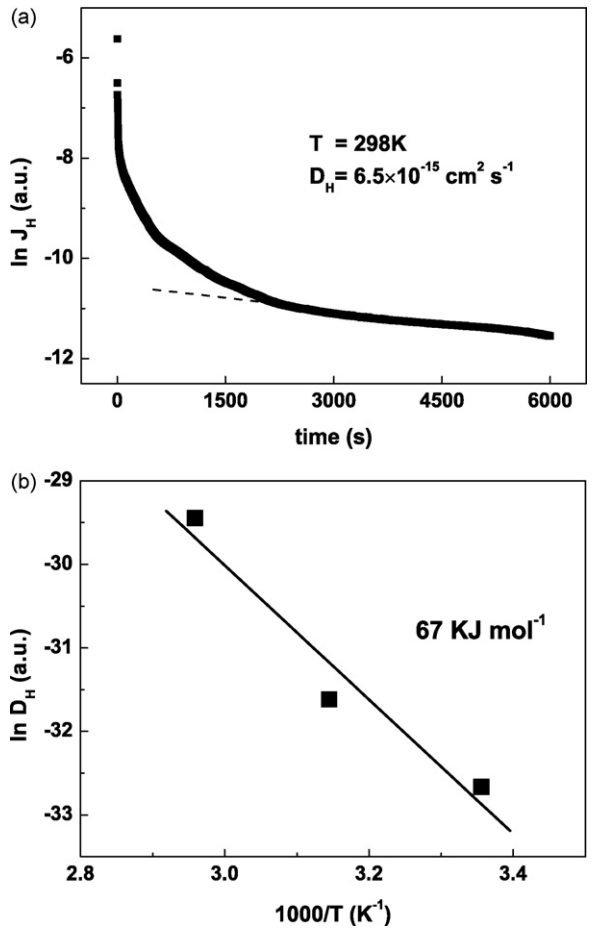

Fig. 7. (a) Hydrogen diffusion coefficient of Mg thin films at room temperature. The dash line is the linear fit according to data. (b) Arrhenius plots of the diffusion coefficients. The straight line is the linear fit according to data.

gen concentration, C^* is the hydrogen concentration after the electrode is anodically biased. Therefore, a plot of $\ln(J_H)$ with respect to the discharge time should be a straight line after a long time with the slope $-\pi^2 D_H t/4L^2$, thus the diffusion coefficient could be calculated. Based on the method mentioned above, the hydrogen diffusion coefficient at 298 K was deduced to be 6.52×10^{-15} cm^2 s^{-1} (Fig. 7(a)), which was little larger than the value $D_H = 1.1 \times 10^{-16}$ cm^2 s^{-1} at 300 K [46]. The faster diffusion rate could be attributed to the catalyst effect of the Pd top layer. The Arrhenius plot of the D_H is shown in Fig. 7(b). The activation energy E_a for hydrogen diffusion was calculated as 67 kJ mol^{-1}, which was about four fifth of the overall activation energy. The smaller activation energy for hydrogen diffusion was beneficial to the application of these samples as smart windows.

4. Conclusions

In summary, we demonstrated the superior hydrogen absorption and desorption properties of Pd-capped Mg films. The samples became transparent and insulating after hydrogenation at 353 K, and reverted to the metallic mirror state completely and rapidly on exposure to air at 298 K. The hydrogen desorption process followed nucleation and growth mechanism and the hydrogen diffusion process was the rate determining step. The hydrogen desorption rates increased at higher temperatures in air and the overall activation energy was 80 kJ mol^{-1}. The diffusion coefficient was calculated as 6.52×10^{-15} cm^2 s^{-1} at 298 K and the corresponding activation energy was deduced to be 67 kJ mol^{-1}. Attributed to the faster diffusion rate and smaller activation energy, the samples exhibited remarkable optical and electrical properties. With the superior hydrogen desorption kinetics at room temperature in air, the Mg films could be candidates for smart windows.

Acknowledgments

The authors acknowledge financial support from the National Natural Science Foundation of China (Nos. 20221101 and 20671004), MOST of China (Nos. 2006AA05Z130 and 2007AA05Z118) and MOE of China (No. 707002).

References

[1] A. Zuttel, L. Schlapbach, Nature 414 (2001) 353–358.
[2] H. Imamura, M. Kusuhara, S. Minami, M. Matsumoto, K. Masanari, Y. Sakata, K. Itoh, T. Fukunaga, Acta Mater. 51 (2003) 6407–6414.
[3] A. Zaluska, L. Zaluski, J.O. Strom-Olsen, J. Alloys Compd. 288 (1999) 217–225.
[4] E. Shalaan, H. Schmitt, Surf. Sci. 600 (2006) 3650–3653.
[5] R. Domenech-Ferrer, M. Gurusamy Sridharan, G. Garcia, F. Pi, J. Rodriguez-Viejo, J. Power Sources 169 (2007) 117–122.
[6] J. Paillier, S. Bouhtiyya, G.G. Ross, L. Roue, Thin Solid Films 500 (2006) 117–123.
[7] H. Akyildiz, M. Ozenbas, T. Ozturk, Int. J. Hydrogen Energy 31 (2006) 1379–1383.
[8] K. Yoshimura, Y. Yamada, M. Okada, Surf. Sci. 566 (2004) 751–754.
[9] A. Leon, E.J. Knystautas, J. Huot, R. Schulz, J. Alloys Compd. 345 (2002) 158–166.
[10] K. Higuchi, H. Kajioka, K. Toiyama, H. Fujii, S. Orimo, Y. Kikuchi, J. Alloys Compd. 293–295 (1999) 484–489.
[11] K. Higuchi, K. Yamamoto, H. Kajioka, K. Toiyama, M. Honda, S. Orimo, H. Fujii, J. Alloys Compd. 330 (2002) 526–530.
[12] N. Bazzanella, R. Checchetto, A. Miotello, Appl. Phys. Lett. 85 (2004) 5212–5214.
[13] A. Leon, E.J. Knystautas, J. Huot, S.L. Russo, C.H. Koch, R. Schulz, J. Alloys Compd. 356 (2003) 530–535.
[14] J.N. Huiberts, R. Griessen, J.H. Rector, R.J. Wijngaarden, J.P. Dekker, D.G. de Groot, N.J. Koeman, Nature 380 (1996) 231–234.
[15] P.V. Sluis, M. Ouwerkerk, P.A. Duine, Appl. Phys. Lett. 70 (1997) 3356–3358.
[16] I.A.M.E. Giebels, J. Isidorsson, R. Griessen, Phys. Rev. B 69 (2004) 205111.
[17] T.J. Richardson, J.L. Slack, R.D. Armitage, R. Kostecki, B. Farangis, M.D. Rubin, Appl. Phys. Lett. 78 (2001) 3047–3049.
[18] S. Bao, K. Tajima, Y. Yamada, M. Okada, K. Yoshimura, Appl. Phys. A-Mater. 87 (2007) 621–624.
[19] D.M. Borsa, A. Baldi, M. Pasturel, H. Schreuders, B. Dam, R. Griessen, P. Vermeulen, P.H.L. Notten, Appl. Phys. Lett. 88 (2006) 241910.
[20] M. Slaman, B. Dam, H. Schreuders, R. Griessen, Int. J. Hydrogen Energy 33 (2008) 1084–1089.
[21] K. Yoshimura, S. Bao, Y. Yamada, M. Okada, Vacuum 80 (2006) 684–687.
[22] K. Tajima, Y. Yamada, S. Bao, M. Okada, K. Yoshimura, J. Appl. Phys. 103 (2008) 013512.
[23] K. Tajima, Y. Yamada, S. Bao, M. Okada, K. Yoshimura, Appl. Phys. Lett. 91 (2007) 051908.
[24] K. Tajima, Y. Yamada, S. Bao, M. Okada, K. Yoshimura, Appl. Phys. Lett. 92 (2008) 041912.
[25] S. Bao, K. Tajima, Y. Yamada, M. Okada, K. Yoshimura, Sol. Energy Mater. Sol. C 92 (2008) 216–223.
[26] K. Yoshimura, Y. Yamada, M. Okada, Appl. Phys. Lett. 81 (2002) 4709–4711.
[27] S. Bao, K. Tajima, Y. Yamada, M. Okada, K. Yoshimura, Sol. Energy Mater. Sol. C 92 (2008) 224–227.
[28] A. Borgschulte, J.H. Rector, H. Schreuders, B. Dam, R. Griessen, Appl. Phys. Lett. 90 (2007) 071912.
[29] K. Yoshimura, S. Nakano, S. Uchinashi, S. Yamaura, H. Kimura, A. Inoue, Meas. Sci. Technol. 18 (2007) 3335–3338.
[30] K. Yamamoto, K. Higuchi, H. Kajioka, H. Sumida, S. Orimo, H. Fujii, J. Alloys Compd. 330 (2002) 352–356.
[31] M. Pasturel, M. Slaman, H. Schreuders, J.H. Rector, D.M. Borsa, B. Dam, R. Griessen, J. Appl. Phys. 100 (2006) 063518.
[32] A. Borgschulte, R. Gremaud, S. Man, R.J. Westerwaal, J.H. Rector, B. Dam, R. Griessen, Appl. Surf. Sci. 253 (2006) 1417–1423.
[33] R. Gremaud, C.P. Broedersz, D.M. Borsa, A. Borgschulte, P. Mauron, H. Schreuders, J.H. Rector, B. Dam, R. Griessen, Adv. Mater. 19 (2007 2813).
[34] S. Bao, Y. Yamada, M. Okada, K. Yoshimura, Appl. Surf. Sci. 253 (2007) 6268–6272.
[35] A. Borgschulte, M. Rode, A. Jacob, J. Schoenes, J. Appl. Phys. 90 (2001) 1147–1154.
[36] T.J. Richardson, J.L. Slack, J.C.W. Locke, S. Seung-Wan, J. Ona, Sol. Energy Mater. Sol. C 90 (2006) 485–490.
[37] M. Pasturel, M. Slaman, D.M. Borsa, H. Schreuders, B. Dam, R. Griessen, W. Lohstroh, A. Borgschulte, Appl. Phys. Lett. 89 (2006) 063518.

[38] A. Borgschulte, R.J. Westerwaal, J.H. Rector, B. Dam, R. Griessen, J. Schoenes, Phys. Rev. B 70 (2004) 155414.
[39] A. Krozer, B. Kasemo, J. Less-Common Met. 160 (1990) 323–342.
[40] P. Hjort, A. Krozer, B. Kasemo, J. Alloys Compd. 234 (1996) L11–L15.
[41] M. Avrami, J. Chem. Phys. 9 (1941) 177–184.
[42] N. Hanada, T. Ichikawa, H. Fujii, J. Phys. Chem. B 109 (2005) 7188–7194.
[43] J.F. Fernandez, C.R. Sanchez, J. Alloys Compd. 340 (2002) 189–198.
[44] H. Hagi, Mater. Trans. JIM 31 (1990) 954–958.
[45] L. Yang, C. Yang-Tse, Int. J. Hydrogen Energy 21 (1996) 281–291.
[46] P. Spatz, H.A. Aebischer, A. Krozer, L. Schlapbach, Z. Phys. Chem. 181 (1993) 393–397.